Investigating the Role of Ammonia in Enhancing Secondary Organic Aerosol Formation from the Co-photooxidation of Anthropogenic and Biogenic VOCs

Yongxin Yan[1], Junling Li[1*], Yufei Song[1], Yushi Gong[1], Shudan Wei[1], Zhaolin Wang[1], Haijie Zhang[1], Yanqin Ren[1], Maofa Ge[2], and Hong Li[1*]

[1] State Key Laboratory of Environmental Criteria and Risk Assessment, Chinese Research Academy of Environmental Sciences, Beijing, 100012, China
[2] Institute of Chemistry, Chinese Academy of Sciences, Beijing, 100190, China

Correspondence to: Hong Li (lihong@craes.org.cn), Junling Li (lijl@craes.org.cn)

Abstract. Ammonia (NH_3) plays a crucial role in the complex physicochemical processes occurring in the atmosphere, but the mechanisms governing secondary organic aerosol (SOA) formation from NH_3-involved interactions between mixed anthropogenic and biogenic organic compounds remain poorly understood, thereby limiting the predictive capacity for air quality and climate. Previous studies have demonstrated that NH_3 can alter the oxidation pathways of single aromatic hydrocarbon precursor, promoting particle formation and growth. However, its role in mixed organic precursor systems has not been systematically explored. This study aims to elucidate these mechanisms through photooxidation experiments conducted in a large outdoor photochemical smog chamber, investigating mixtures of n-heptylcyclohexane (anthropogenic) and α-pinene (biogenic) under varying NH_3 conditions. The results indicated that NH_3 obviously accelerated VOC degradation and significantly contributed to SOA enhancement through facilitating nucleation and participating in particle-phase reactions in the mixed system. The presence of NH_3 could not only promote the generation of intermediates such as aldehydes and ketones, but also lead to an increase in SOA mass and number concentration, particularly nitrogen-containing light-absorbing substances like imidazoles. This research can provide a scientific basis for systematically assessing how NH_3 affects the co-oxidation of ambient anthropogenic and biogenic gases, and deepen the understanding of its role in SOA generation, particularly light-absorbing aerosols, in the AVOC-BVOC mixed system.

1 Introduction

The atmospheric photochemical oxidation of anthropogenic and biogenic volatile organic compounds (AVOCs, BVOCs) can lead to the formation of secondary organic aerosols (SOA), which have been widely considered important for atmospheric chemistry, global climate, and human health (Ziemann and Atkinson, 2012; Shrivastava et al., 2017; Liu et al., 2022). Recent laboratory experiments have demonstrated that the contribution of specific VOC species to SOA varies under different conditions, including oxidant species and concentrations, seed particles, inorganic gas, temperature, relative humidity, and radiation intensity (Zhang et al., 2019; Palm et al., 2017; Zhang et al., 2023; Li et al., 2021a). Nevertheless, the evidence that

current model predictions of SOA are generally lower than field observations suggests that significant nonlinear effects occur in the formation of SOA in the mixed VOCs systems (Hallquist et al., 2009; Xu et al., 2021). Hence, knowledge gaps still persist regarding the complex oxidation mechanisms of multiple coexisting gas- and particle-phase substances in the atmosphere, along with the properties, composition, and formation mechanisms of the resulting SOA, which poses
35 challenges for precisely evaluating the global SOA budget, origins, and climatic implications.

It is well known that ammonia (NH_3) is a common primary alkaline pollutant in the atmosphere, primarily emitted from agricultural sources. Moreover, on-road mobile sources of NH_3 are becoming increasingly important with the rise in urban automobile ownership (Sun et al., 2017), significantly contributing to the pollution levels of fine particulate matter ($PM_{2.5}$) (Wen et al., 2023). Recent studies have revealed that NH_3 can influence the formation and chemical composition of single
40 VOC-derived SOA (Du et al., 2023). NH_3 can promote new particle formation (NPF) and particulate growth during the photo-oxidation of aromatic hydrocarbons (e.g., toluene and xylene) (Liu et al., 2021a). Additionally, NH_3 directly contributes to SOA formation through acid-base reactions with organic compounds during the photo-oxidation of biogenic olefins (e.g., α-pinene) (Hao et al., 2020). Tunnel measurements show that NH_3 emitted by traffic rose from 21~225 ppb at the entrance to 40~2776 ppb at the exit (Liu et al., 2014). Therefore, investigating the role of high concentration NH_3 in the
45 photochemical oxidation of mixed VOCs would benefit to deepen our understanding of the complex atmospheric oxidation mechanisms.

In recent years, the relative contribution of SOA to $PM_{2.5}$ mass concentration has significantly increased (Ming et al., 2017). Long chain alkanes have been found to not only significantly affect the SOA yield, but also play an important role in atmospheric oxidation (Donahue et al., 2009; Tang et al., 2019). Long chain alkanes in the atmosphere come from a wide
50 range of sources, including volatile chemicals such as coatings and exhaust emissions from motor vehicles (Fang et al., 2021; Wang et al., 2021a; Qi et al., 2019; Deng et al., 2017b). Research has shown that the amount of SOA generated by long-chain alkanes is comparable to that of polycyclic aromatic hydrocarbons and monocyclic aromatic hydrocarbons, and even more significant in some cases (Luo et al., 2019; Agrawal et al., 2008; Siegl et al., 1999; Yuan et al., 2013; Deng et al., 2017a). The photochemical reactivity and SOA generation potential of long-chain alkanes are greatly influenced by their
55 chemical structural characteristics. Cycloalkanes have the highest activity and SOA generation potential, followed by branched alkanes, and finally straight chain alkanes (Hu et al., 2022). As a mixed hydrocarbon compound with both cyclic and branched alkyl structures, n-heptylcyclohexane can provide important references and inspirations for the research of other long-chain alkanes. On a global scale, the BVOC emissions account for over 90% of the total VOCs worldwide (Shao et al., 2022; Ahlberg et al., 2017), making them the most important source of atmospheric organic compounds and a
60 significant contributor to global SOA production (Chen and Jang, 2012). Under real atmospheric conditions, when BVOCs are mixed with anthropogenic emissions, their oxidation pathways and potential for generating SOA can be altered (Donahue et al., 2006; Emanuelsson et al., 2013; John H. Offenberg et al., 2007; Voliotis et al., 2021; Li et al., 2022b). Among them, α-pinene has the characteristics of high emissions, high reactivity, and high SOA contribution, making it a very important BVOCs species in the atmospheric environment (Wang et al., 2021b). At present, our understanding of the mixed oxidation

65 mechanism of biogenic olefins and long-chain alkanes, as well as their derived SOA components and properties, is still limited. Moreover, there is less research on the impact of NH_3 on AVOC-BVOC mixed systems, and the mechanism of SOA formation in these systems is not yet clear.

Herein, a large outdoor photochemical smog chamber simulation was conducted to explore the SOA formation from the mixed system of n-heptylcyclohexane (representing AVOCs) and α-pinene (representing BVOCs) under the presence of NH_3.

70 Then an in-depth analysis of the SOA composition was conducted, further clarifying the potential chemical mechanisms. This study aims to comprehensively reveal the important enhancing role of NH_3 on the co-photooxidation of anthropogenic-biogenic mixed system, and furtherly improve the understanding of the mechanisms and influencing factors of SOA in the system.

2 Materials and Methods

75 ### 2.1 Experimental conditions

The experiments were conducted in a large outdoor photochemical smog chamber located on one rooftop of the building at the Chinese Research Academy of Environmental Sciences (CRAES). It was a 56 m^3 Teflon chamber covered with a well-controlled enclosure, inside where three fans were fixed to ensure uniform mixing (Li et al., 2021b). Before each experiment, the chamber was purged with zero air at a flow rate of 100 L min^{-1} for at least 24 hours to ensure cleanliness. Herein, all the

80 experiments were performed from October to the ensuing January, and the initial conditions and experimental results could be found in Table S1. As significant organic precursors of SOA, the liquid-phase n-heptylcyclohexane, and/or α-pinene with known volumes were injected into a U-shaped tube and then blown into the chamber with zero air after heating. In all experiments, the initial concentration of n-heptylcyclohexane (TCI Development Co., Ltd, Shanghai) was in the range of 49.0~119.8 ppb, while α-pinene (Beijing Inno Chem Science & Technology Co., Ltd) was in the range of 43.7~86.7 ppb.

85 With HONO as the precursor for OH radicals and NO, it was prepared by the dropwise addition of 0.2 mL 5 wt % $NaNO_2$ into 0.4 mL 30 wt % H_2SO_4, formed NO, NO_2, and HONO from which were blown into the chamber by zero air likewise. The measured initial NOx concentration in the chamber ranged from 89.9 to 157 ppb. NH_3 was introduced from a 500 ppm standard gas cylinder, the concentration of which was calculated based on the chamber volume and added volume of NH_3. The initial NH_3 concentration was in the range of 74.85~748.5 ppb. When the target species that introduced into the chamber

90 were thoroughly mixed, the enclosure was opened, thus the photochemical reaction began. The entire photochemical reaction process of each experiment lasted about 7 h (usually from 10 a.m. to 17 p.m.), with a maximum temperature (T) of 14.4~40.7 ℃ and a maximum relative humidity (RH) of less than 15% inside the chamber. The sunlight was utilized as the natural light source at JNO_2 of 0.9~4.4 ×10^3 s^{-1}. The first 3.5 hours of the reaction process were defined as the former half of the experiment and the second 3.5 hours as the latter half of the experiment. Each set of experiments was conducted at least 2

95 times to verify reproducibility and ensure robust results. Under background conditions, the chamber air contained SO_2≤0.5 ppb, NOx≤2 ppb, and O_3≤0.5 ppb, while released or formed VOCs and particles were negligible (<0.01 µg m^{-3}).

2.2 Instrumentation

The collected precursor samples (n-heptylcyclohexane and α-pinene) in the Tenax TA tube underwent quantitative analysis
using thermal desorption gas chromatography (TD-GC, GC, 8890, Agilent, USA; TD, UNITY-xr, Germany) to obtain
100 precursor concentrations and consumption rates within the chamber. The mass concentration, number concentration, surface
mean diameter, and volume concentration of formed particles were monitored with a scanning mobility particle sizer (SMPS,
model 3080, model 3081, and model 3772, TSI Inc., USA). Additionally, the qualitative analysis of organic chemical
compounds, which were subjected to ultrasonic extraction from quartz films using 10 mL of methanol (20 minutes), was
performed using an electrospray ionization quadrupole time-of-flight mass spectrometer (ESI-Q-ToF-MS, Bruker, Germany).
105 Furthermore, an FTIR spectrometer (Bruker, Germany) equipped with a RTDLaTGs detector and a UV-Vis light
spectrometer (Hitachi, U-3900) were applied to the qualitative detection of potential functional groups in the organic
components. The qualitative and quantitative analysis of eluted aldehyde-ketones from collected samples were carried out
using an HPLC-UV/MS (Shimadzu, Japan). The T and RH inside the chamber were monitored using the temperature and
humidity sensors (Beijing Star Sensor Technology Co., Ltd.), while the irradiance was detected with a JNO_2 filter radiometer
110 (Metcon, Germany). The consumption and generation of gaseous NOx and O_3 inside the chamber were monitored in real-
time by NOx (EC 9841, Ecotech, Australia) and O_3 analyzers (EC 9830, Ecotech, Australia).

2.3 Calculation

In this work, the OH exposure during the photo-oxidation process of precursor compounds were quantified by utilizing TD-
GC, as illustrated by Eq. (S1) (Mao et al., 2009):

115 $$OH\ exposure = \frac{ln\frac{[tracer]_0}{[tracer]_t}}{k}, \qquad (S1)$$

where k denoted the rate constant for the reaction of the tracer and the OH radical.

Here, the tracer referred to a precursor compound capable of reacting with OH radicals. Given the rapid photo-oxidation rate
of α-pinene, n-heptylcyclohexane was appointed as the trace. In experiments without n-heptylcyclohexane, α-pinene served
as the tracer. At the standard temperature (298 K), the reaction rate constant for OH radical with n-heptylcyclohexane was
120 1.91×10^{-11} cm^3 $molecules^{-1}$ s^{-1}, and with α-pinene was 5.23×10^{-11} cm^3 $molecules^{-1}$ s^{-1} (Atkinson and Arey, 2003).
Furthermore, the physical significance of OH exposure was the total OH concentration from the onset to the detection period;
hence, the cumulative time was employed in the calculation of OH exposure.

The SOA yield (Y) was defined as the fraction of reactive organic gases (ROG, µg m^{-3}) converted into aerosols, and it could
be calculated by Eq. (S2):

125 $$Y = \frac{\Delta Mo}{\Delta ROG}, \qquad (S2)$$

where ΔMo (µg m^{-3}) was the maximum mass concentration of SOA, obtained by deriving the data from the Scanning
Mobility Particle Sizer (SMPS); ΔROG is the amount of precursor substances involved in the reaction.

The absorption of SOA generated in the experiment across the 300 to 700 nm was measured using a UV-Vis absorption spectrophotometer. The specific absorption coefficient, denoted as Abs_λ, was calculated based on Eq. (S3) (Liu et al., 2021b):

130 $$Abs_\lambda = (A_\lambda - A_{700}) \cdot \frac{V_1}{V_a \cdot L} \cdot ln10, \qquad \text{(S3)}$$

where A_λ was the light absorption coefficient of SOA at the λ wavelength, A_{700} was the light absorption intensity background value, V_1 was the volume of methanol with dissolved aerosols, V_a was the volume of the sampled air, and L (1 cm) was the optical path length.

Based on the UV-Vis absorption spectra, the mass absorption efficiency (MAE_λ; m^2 g^{-1}) was characterized the ultraviolet

135 absorption intensity of SOA, which was calculated according to Eq. (S4) (Liu et al., 2021b):

$$MAE_\lambda = \frac{Abs_\lambda}{M}, \qquad \text{(S4)}$$

where Abs_λ (m^{-1}) was the light absorption coefficient of SOA at the λ wavelength, and M (μg m^{-3}) was the mass concentration of methanol-soluble organic matter.

Mass defect was defined as the difference between exact mass and nominal mass of a certain compound (Roach et al., 2011).

140 ## 3 Results and discussion

3.1 General results

The experiments were carried out according to the scheme of n–heptylcyclohexane + HONO (AL), n–heptylcyclohexane + HONO + NH_3 (AL-N), α–pinene + HONO (AP), α–pinene + HONO + NH_3 (AP-N), n–heptylcyclohexane + α–pinene + HONO (MIX) and n–heptylcyclohexane + α–pinene + HONO + NH_3 (MIX-N), and the initial conditions and results were

145 summarized in Table S1. In the background experiment, the mass concentration of inorganic particles formed from the photochemical reaction of NH_3 with NOx was below 10 μg m^{-3}, and the number concentration was < 2000 # cm^{-3} (Figure S1). This is approximately 1~2 orders of magnitude lower than the total particle concentration in the organic reaction system. Therefore, the contribution of inorganic particle formation in the organic precursor system is considered negligible. As showed in Fig.1(a), the maximum of OH exposure was in the range of (5.6~7.9) × 10^{10} molecules^{-1} cm^{-3} s corresponding to

150 10.4~14.6 simulated hours, assuming a diurnal average OH concentration of 1.5×10^6 molecules^{-1} cm^{-3} (Mao et al., 2009; Li et al., 2024). The OH exposure continuously increased over time, leading to an enhanced atmospheric oxidation capacity. The reaction commenced with a decline in the concentration of reactants, and the consumption rate of which seemed to be accelerated by the addition of NH_3 (Fig. 1(b)). Upon illumination, the SOA mass concentration rose rapidly while NOx levels declined. Compared with the NH_3-free system, the NH_3-containing system produced significantly higher SOA mass

155 concentrations; moreover, the mixed organic system yielded higher SOA mass concentrations than the single one.
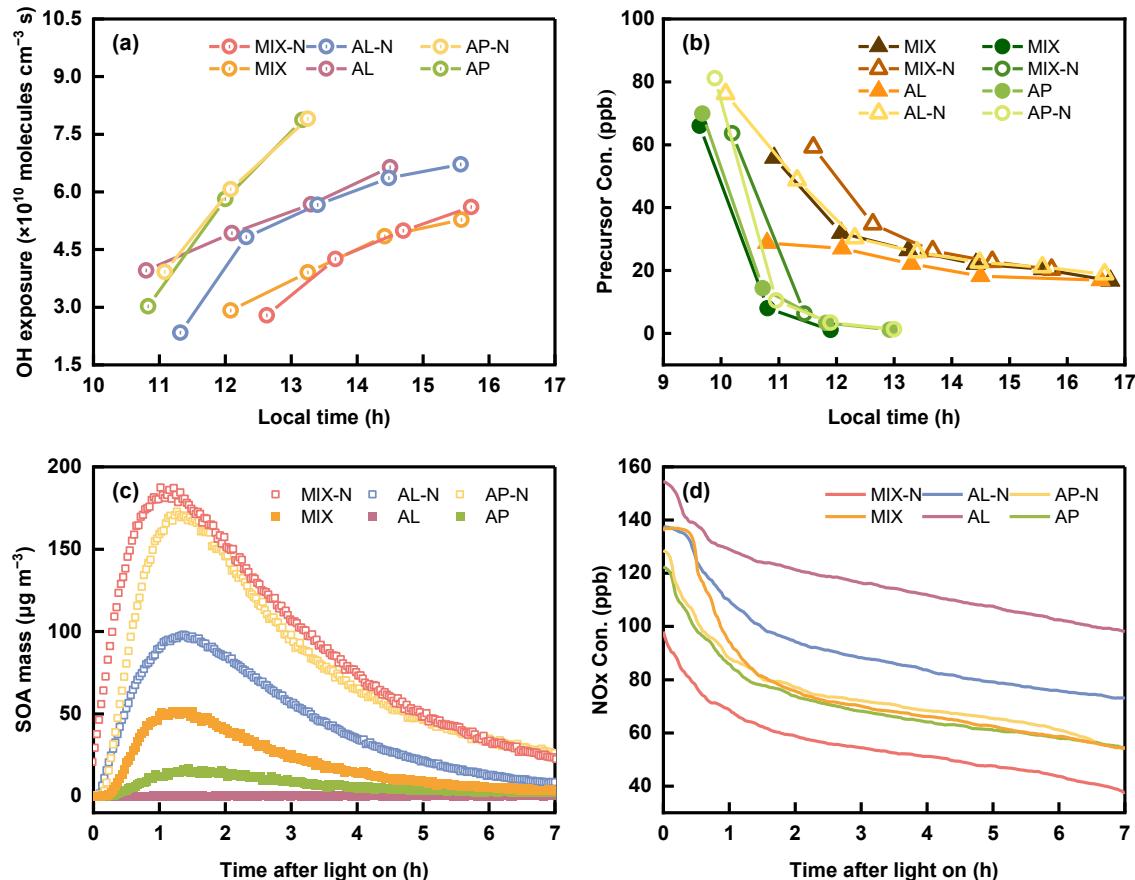
Figure 1: (a) The OH exposure (b) Precursor concentration (c) SOA mass concentration and (d) NOx concentration in the MIX-N (n-heptylcyclohexane + α-pinene + HONO + NH₃) experiment, MIX (n-heptylcyclohexane + α-pinene + HONO) experiment, AL-N (n-heptylcyclohexane + HONO + NH₃) , AL (n-heptylcyclohexane + HONO) experiment, AP-N (α-pinene + HONO + NH₃) experiment and AP (α-pinene + HONO) experiment. In Fig.1(b), the triangle represented n-heptylcyclohexane, and the circle referred to α-pinene. In Fig(b) and (c), the solid and hollow symbols denoted NH₃-free and NH₃-containing experimental systems, respectively.

In terms of particle size, the average SOA diameter in the MIX-N experiment was distinctly larger than that in the AL-N experiment but almost identical to that in the AP-N experiment, implying that the disparity stemmed primarily from precursor type rather than NH₃. Previous work likewise indicated that the average SOA diameter in mixed systems was governed by the highly reactive BVOC precursors (Cui et al., 2024). As showed in Fig.2, the average diameter of particles from photochemical oxidation ranged from 300 to 450 nm in the MIX-N and MIX experiment, ranged from 200 to 300 nm in the AL-N and AL experiment, and ranged from 250 to 450 nm in the AP-N and AP experiment. Obviously, the absence of any appreciable shift in average diameter between NH₃-present and NH₃-free conditions further corroborated that NH₃ exerted no significant enhancement on particle size. However, Li et al. (2018) reported that NH₃ could increase SOA size-growth potential; this discrepancy was attributable to their lower VOC/NOx ratio (1.6~4.9 ppbC ppb⁻¹). Under such high-

NOx conditions, the photo-oxidation of organics preferentially drove post-nucleation growth, an effect that was largely muted in our experiments with higher VOC/NOx (3.1~16.2 ppbC ppb^{-1}) (Li et al., 2018; Li et al., 2022c).
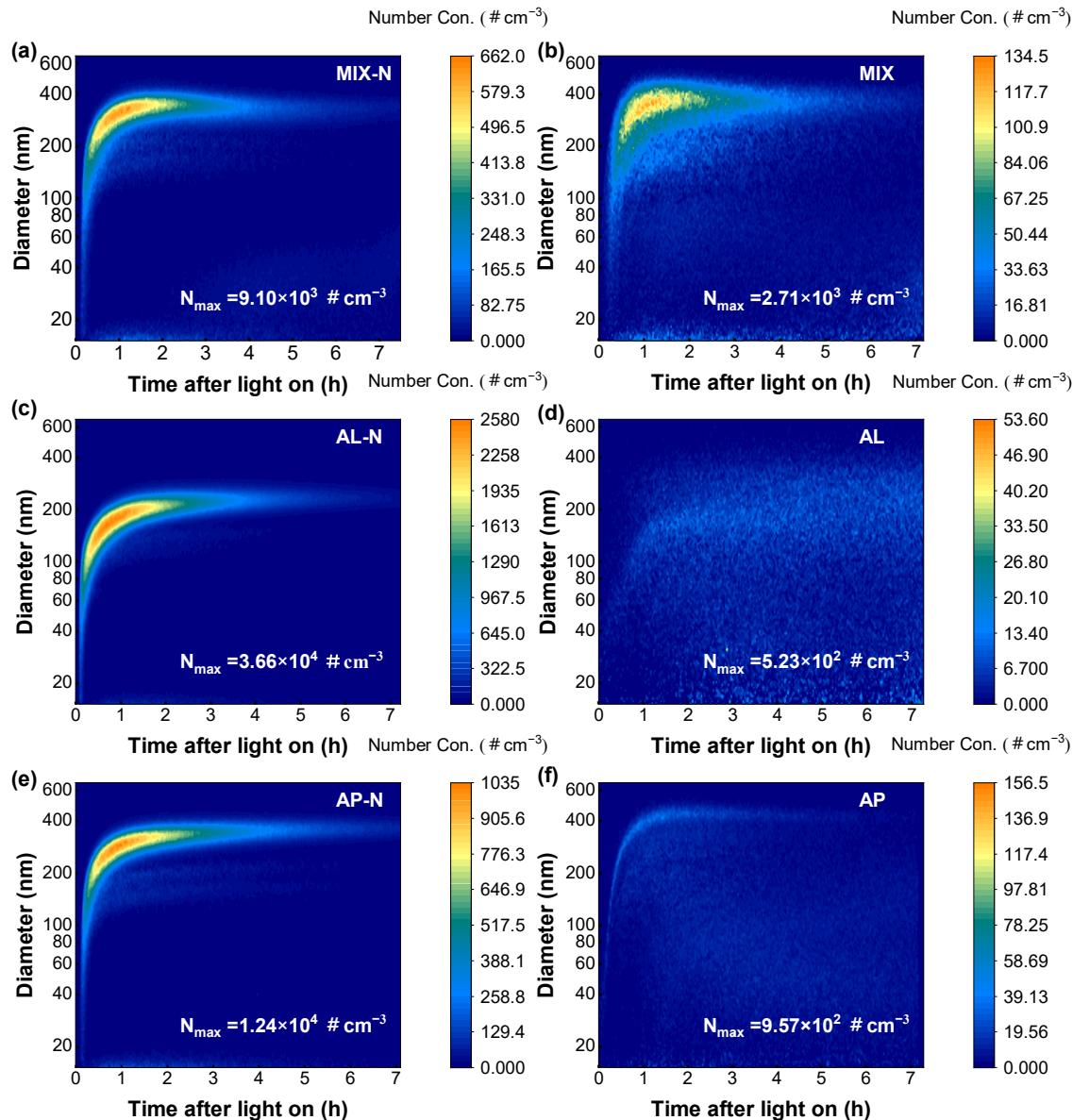
Figure 2: The number concentration distributions of particles at different diameters in the (a) MIX-N (n-heptylcyclohexane + α-pinene + HONO + NH₃) experiment, (b) MIX (n-heptylcyclohexane + α-pinene + HONO) experiment, (c) AL-N (n-heptylcyclohexane + HONO + NH₃) , (d) AL (n-heptylcyclohexane + HONO) experiment, (e) AP-N (α-pinene + HONO + NH₃) experiment and (f) AP (α-pinene + HONO) experiment.

In the process of each experiment, particles were generated rapidly within the first hour of the reaction (Fig. 2). When the maximum number concentration reached approximately 10^4 # cm^{-3}, strong particle growth appeared as a clear banana shape. Compared to the NH₃-free experiments, the maximum SOA yield of the mixed organic system rose from 14.3 % to 40 %

when NH_3 was present, indicating that the introduction of NH_3 led to a marked escalation in SOA production (Fig. 3(a)). Although temperature could significantly affect the partitioning process of organic compounds and lower temperatures could sensibly facilitated the formation of particles (Li et al., 2022d), the particle mass concentration exhibited a pronounced

185 enhancement in the NH_3-present systems under identical organic precursor as well as comparable temperature and the reactive organic compounds-to-primary NOx concentration ratio (VOC/NOx), suggesting that NH_3 played a facilitative role in the particle formation aligned with other research (Xu et al., 2021). It was probably because NH_3 could react with certain compounds found in SOA, contributing to convert itself into nitrogen-containing organic compounds (NOC) that remained in particles (Laskin et al., 2015), such as imines and (O'brien et al., 2013). On the other hand, both nuclei coagulation and

190 condensation caused by acid–base reactions between NH_3 and organic acids (such as pinic acid and pinonic acid) were responsible for the SOA growth (Xu et al., 2021).
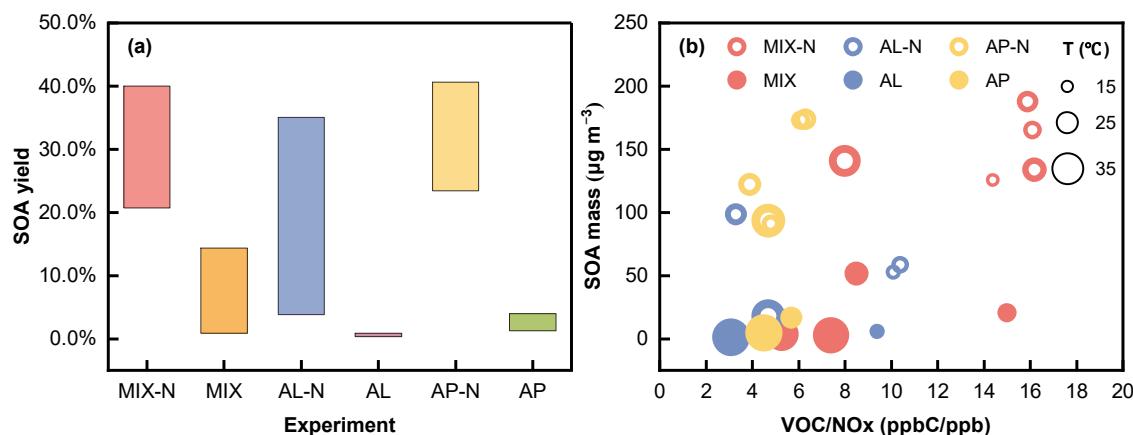
Figure 3. The (a) SOA yield and (b) relationship between SOA formation and NH_3, VOC/NOx ratio, as well as temperature (T) in the MIX-N (n-heptylcyclohexane + α-pinene + HONO + NH_3) experiment, MIX (n-heptylcyclohexane + α-pinene + HONO)
195 experiment, AL-N (n-heptylcyclohexane + HONO + NH_3), AL (n-heptylcyclohexane + HONO) experiment, AP-N (α-pinene + HONO + NH_3) experiment and AP (α-pinene + HONO) experiment. In Fig. 3(b), the temperature and SOA mass concentration here referred to the maximum value during the reaction process. The red circles referred to MIX-N experiments, and the red filled circles referred to MIX experiments. The blue circles referred to AL-N experiments, and the blue filled circles referred to AL experiments. The yellow circles referred to AP-N experiments, and the yellow filled circles referred to AP experiments. The size of
200 the circle represented the level of temperature. The larger the circle, the higher the experimental temperature.

3.2 Light absorption of SOA

Identifying the chemical class of SOA was essential to elucidating how NH_3 influences the photo-oxidation of binary organic mixtures; to this end, we derived functional group information of the SOA by resolving the absorption spectrum. The infrared absorption spectrum featured peaks that correspond to the functional groups of organic matter in the SOA. Various
205 characteristic functional groups of the main products could be differentiated by identifying the positions of these peaks (Fig. 4). The peak observed at 2923 cm^{-1} and 2855 cm^{-1} originated from the O–H stretching vibration. The characteristic peak at 1645 cm^{-1} corresponded to the C=O stretching vibrations of the carbonyl group in either aldehyde or amide. The peak around 1054 cm^{-1} was considered as the O—H bending vibration or C—O stretching vibration, while the distinctive peak at

1382 cm^{-1} represented the —NO$_2$ stretching vibration of the nitro group (Babar et al., 2017; Huang et al., 2018). These peaks
210   were consistently found in both MIX-N, AL-N and AP-N experiments, indicating that the predominant products from the
NH$_3$-containing systems were compounds with carbonyl functionalities, along with certain NOC (Liu et al., 2015).
Especially in systems containing NH$_3$, the enhanced peak at 1382 cm^{-1} suggested that the introduction of NH$_3$ led to an
increased light absorption of SOA, resulting from the enhancement of NOC formation (Wang et al., 2022).

In the UV absorption profiles, the peak at 300 nm was found when NH$_3$ participating in the reaction, which suggested the
215   formation of carbonyl groups (Martinez et al., 1992). However, the MAE in each system were relatively small, and the light
absorption within the UV-visible spectrum were weak. This could be attributed to the absence of conjugated double bonds in
the SOA derived from n-heptylcyclohexane and α-pinene (Lambe et al., 2012). Notably, the latter phase of each experiment
showed a more pronounced light absorption than the former phase. The MAE at 300 nm during the former half of the
experiments followed the sequence MIX-N > AL-N > AP-N, whereas followed MIX-N ≈ AP-N > AL-N in the latter half.
220   These observations implied that more light-absorbing substances generated as the reaction progressed. Furthermore, the SOA
generated from the n-heptylcyclohexane and α-pinene mixture contained a higher concentration of light-absorbing
substances per unit mass.
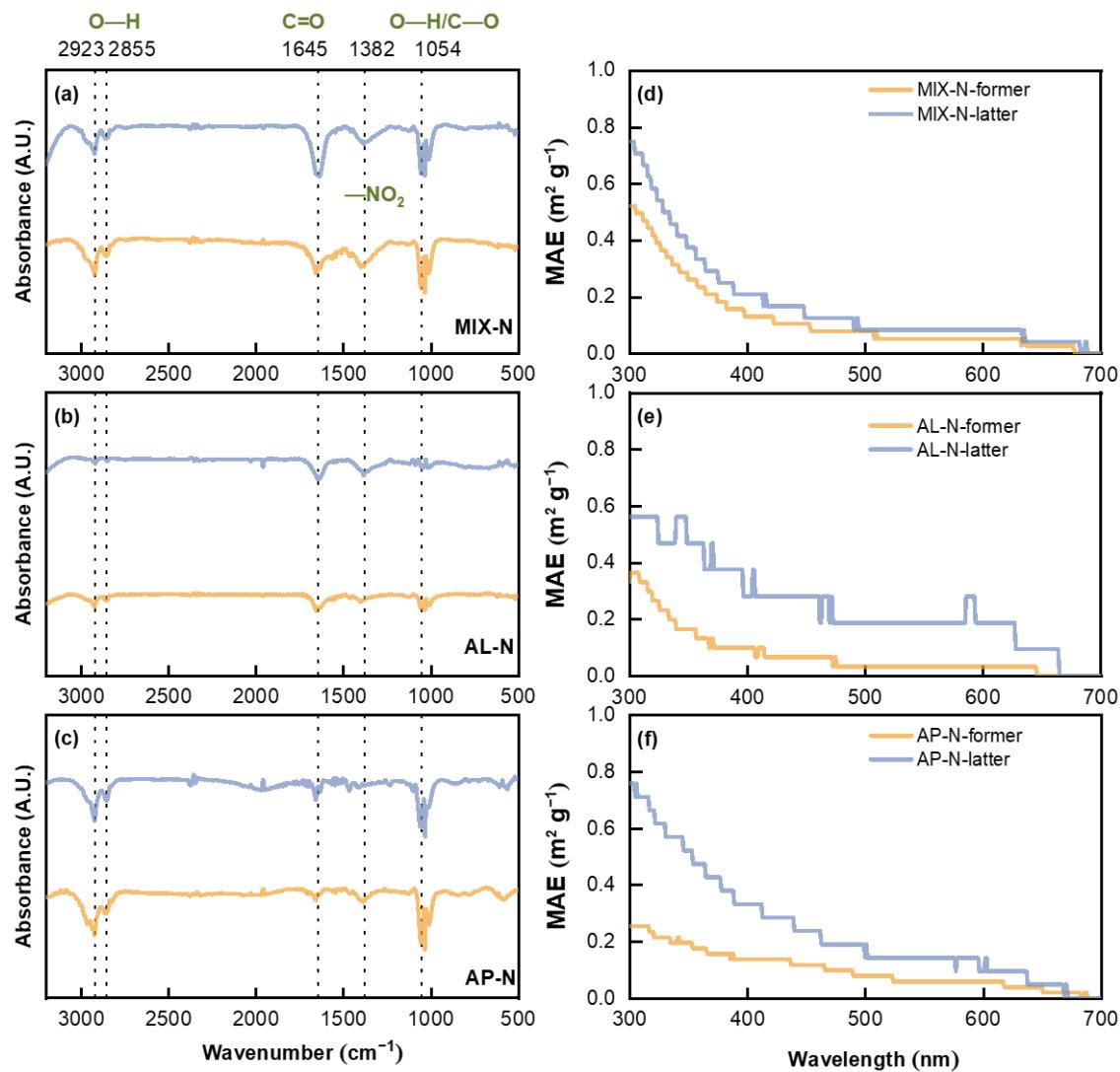
Figure 4. Infrared absorption spectrogram of generated particles in the (a) MIX-N (n-heptylcyclohexane + α-pinene + HONO + NH₃) experiment, (b) AL-N (n-heptylcyclohexane + HONO + NH₃), (c) AP-N (α-pinene + HONO + NH₃) experiment and ultraviolet absorption spectrogram of generated particles in the (d) MIX-N (n-heptylcyclohexane + α-pinene + HONO + NH₃) experiment, (e) AL-N (n-heptylcyclohexane + HONO + NH₃), (f) AP-N (α-pinene + HONO + NH₃) experiment. "Former" referred to the former half of the reaction process, and "Latter" referred to the latter half of the reaction process.

3.3 Chemical compositions of SOA

3.3.1 Molecular composition

For a deeper examination on the characteristics of organic compounds within the particulate phase, mass spectrometry was utilized to analyse the particulate matter under both positive and negative ionization modes, as shown in Fig. 5. Under positive mode, a notable formation of trimer was observed in both NH₃-containing and NH₃-free mixed system, with m/z

spanning ranges of 0~300 Da, 300~450 Da, and 500~550 Da. However, the signal intensity of SOA polymeric products

235 slightly decreased in the NH₃-containing mixed system, indicating that participation of NH₃ in photochemical reactions may have competitively interrupted the cross-reactions between n-heptylcyclohexane and α-pinene and their intermediates, thereby suppressing the formation of high-molecular-weight organics to some extent.
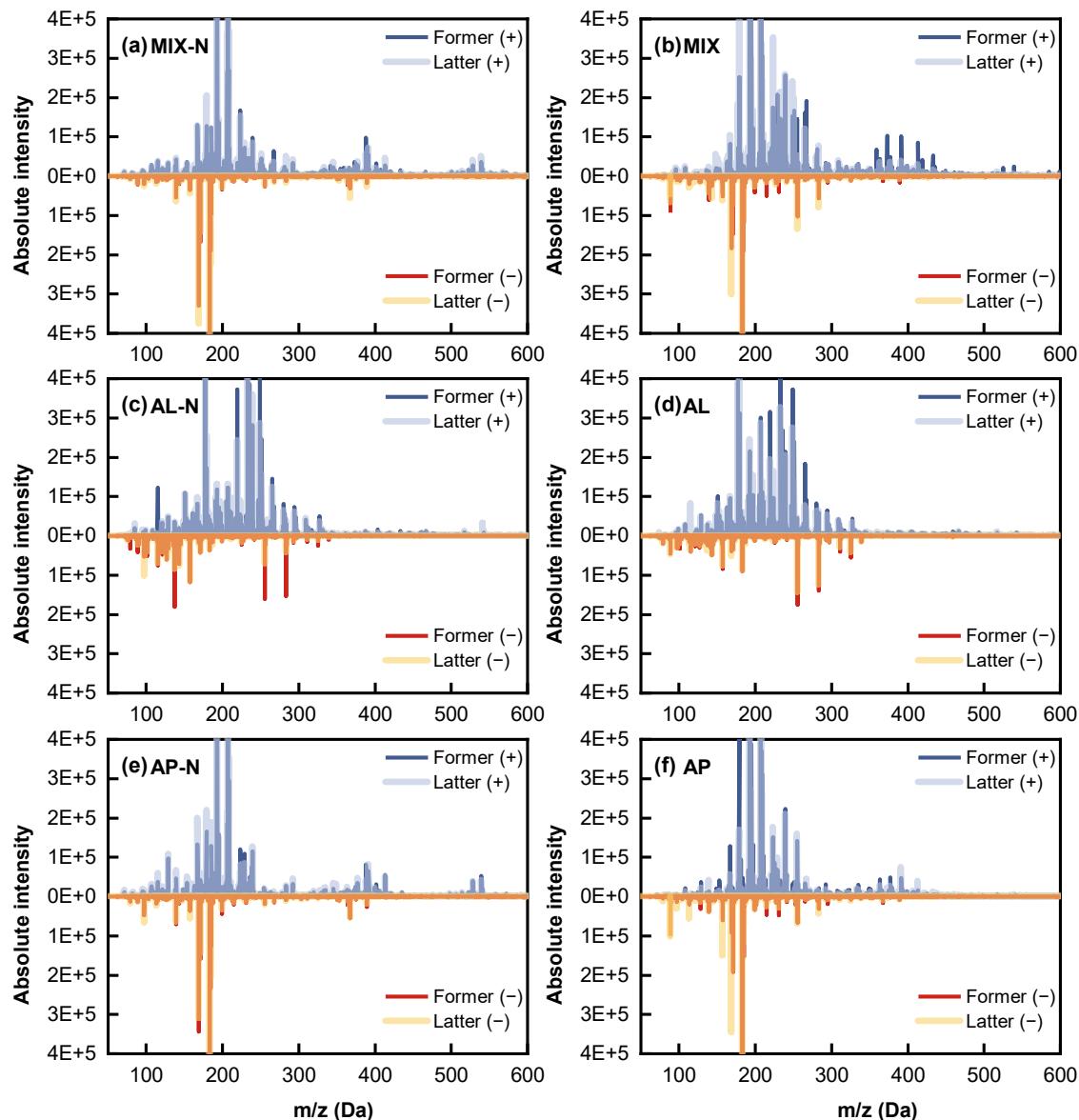
Figure 5. Mass spectra of generated SOA under positive (+) / negative (−) mode in the (a) MIX-N (n-heptylcyclohexane + α-pinene
240 **+ HONO + NH₃) experiment, (b) MIX (n-heptylcyclohexane + α-pinene + HONO) experiment, (c) AL-N (n-heptylcyclohexane + HONO + NH₃), (d) AL (n-heptylcyclohexane + HONO) experiment, (e) AP-N (α-pinene + HONO + NH₃) experiment and (f) AP (α-pinene + HONO) experiment.**

As Venn diagram displayed in the Fig. 6, the positive mode revealed a higher detection of compounds with mass spectrometry signal relative intensities exceeding 0.05 compared to the negative mode, with a limited overlap in compound

245   detection between the two modes. This indicated a prevalence of compounds with protonatable functional groups (such as —NH—, —O—, —CH$_2$, C=O, etc.) in the reaction systems involving n-heptylcyclohexane and α-pinene, while compounds with alcoholic and carboxylic acid functionalities were relatively less abundant (Glasius, 1999, J. Chromatogr. A; Steckel and Schlosser, 2019, Molecules). In positive mode, 414 compounds were totally detected, with 234 compounds consistently present across both former and latter half of the reaction, representing over 56% of the total compounds identified (Table S2).

250   In negative mode, 182 compounds were totally identified, with 74% of these compounds being consistently detected throughout the reaction phases. The presence of unique compounds in each stage, observed in both ionization modes, was likely due to the cross-reactions of intermediates thus the generation of new substances (Shao et al., 2022).
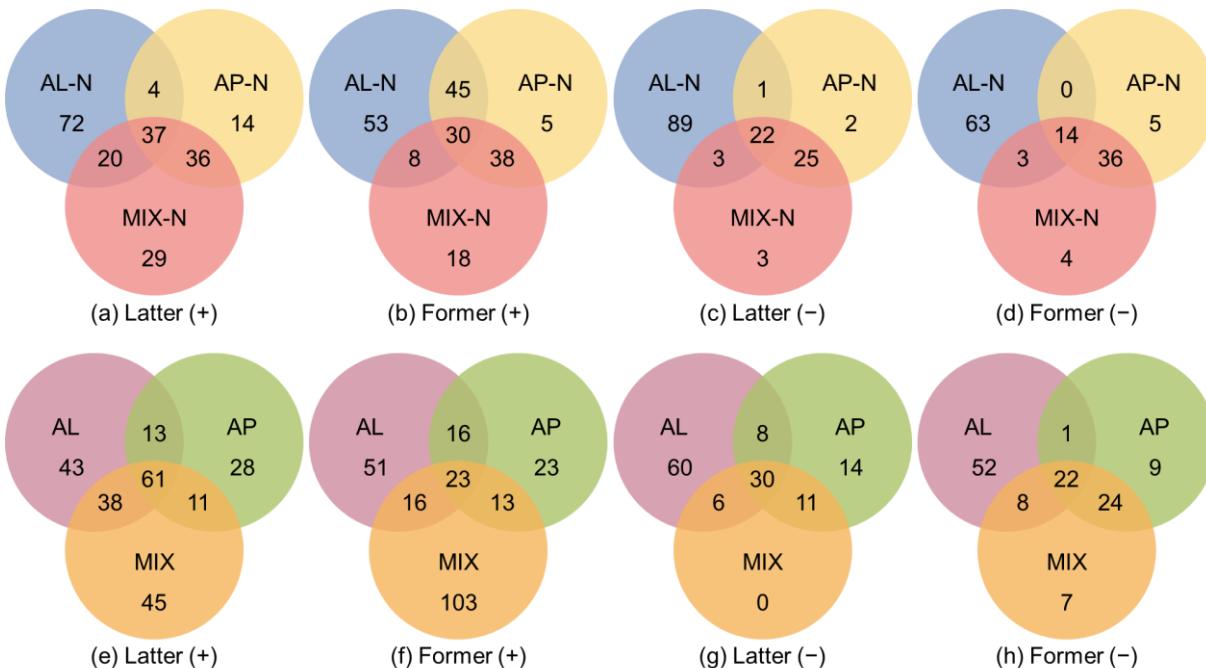
Figure 6. Number of common discrete compounds and unique compounds in single and mixed experiments detected under positive
255   **(+) and negative (−) mode, the signal relative intensity of which were greater than 0.05. A relative intensity of 1 was assigned to the most intense peak that was non-impurity in each sample group.**

In the presence of NH$_3$ within the reaction system, the species common to both the MIX experiments and the AP experiments were 1.8 to 12 times more abundant than those common to the MIX experiments and the AL experiments. This finding was similar to the 16-fold increase reported by Shao et al. (2022) in their experiments with mixed α-pinene and o-

260   cresol, underscoring the prominence of α-pinene oxidation in mixed systems of AVOC and BVOC. Conversely, in the absence of NH$_3$, a higher number of shared compounds between the AL and MIX experiments were noted in positive mode, whereas a greater overlap was observed between the AP and MIX experiments in negative mode, indicating that the

participation of NH_3 could promote the formation of a greater number of compounds bearing readily protonatable functional groups.

3.3.2 Elementary composition

An in-depth analysis of the SOA chemical composition across the systems was performed by categorizing the detected molecular formulas according to their elemental makeup, primarily into CHO and CHON groups (with C, H, O, N corresponding to the constituent atoms in the molecules), and further divided into six classes based on carbon count. The observed peak area for each compound was normalized against the total peak area of the sample, as illustrated in Fig. 7. Among molecules containing solely C, H, and O, $C_3\sim C_5$ exhibited lower signal intensities. The MIX-N experiment predominantly comprised $C_6\sim C_{10}$, whereas the MIX experiment was enriched with $C_{11}\sim C_{15}$ molecules. This served as compelling evidence that the presence of NH_3 strongly promoted the termination of cross-reactions or self-oxidation of organic precursors and their intermediates, thereby suppressing the formation of high-molecular-weight compounds. For molecules that include C, H, O, and N, the majority in each system were composed of compounds with 9 to 10 carbon atoms.
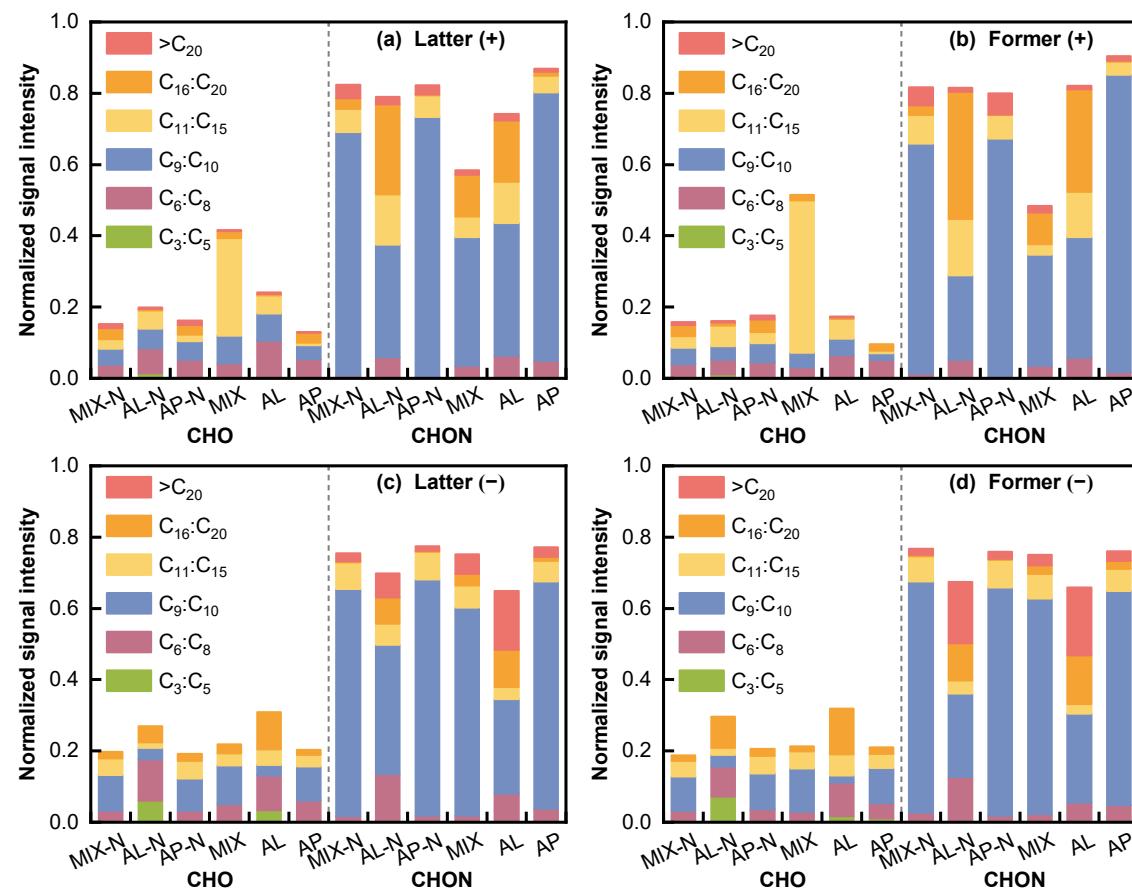
Figure 7. The normalized signal intensity distribution of different compound categories (CHO and CHON) for various single and mixed precursor systems in positive and negative mode.

C_6~C_{10} compounds included those produced through both functionalization (addition oxygenated function group) and fragmentation (cleavage of C—C bond) pathways during α-pinene oxidation (Eddingsaas et al, 2012). The main routes of the α-pinene degradation were the OH addition channel and an H-abstraction channel (Capouet et al., 2004), via which particle-phase dimerization and oligomerization reactions finally occurred (e.g. alcohol + carbonyl to form hemiacetals and acetals, hydroperoxide + carbonyl to form peroxyhemiacetals and peroxyacetals, carboxylic acid + alcohol to form esters, and aldehyde self-reactions to form aldols) (Ziemann and Atkinson, 2012; Gao et al., 2004a, b), resulting in formation of large molecules (>C_{10}) and potentially accounting for the C_{16}~C_{20} abundance. Additionally, the gas-phase autoxidation of α-pinene might contribute to the formation of CHO products with 16~20 carbon atoms (Berndt, 2021; Ehn et al., 2014).

In general, the heptyl-chain of n-heptylcyclohexane could afford it many sites of reaction without the potential of disrupting the stability of the C_6 ring, and continued oxidation of branch chain would tend to eventually cause fragmentation (Capouet et al., 2004). This could account for the predominant presence of C_3~C_5 in AL experiments, which was likely associated with the oxidation of the branched structure of n- heptylcyclohexane. Obviously, the presence of NH3 led to a significant enhancement in the abundance of C_3~C_5 molecules, as NH_3 could promote the partitioning of these small molecules from the gas phase into the particulate phase (Li et al., 2022a).

In the MIX experiments, products containing only CHO elements exhibited a higher abundance of C_{11} to C_{15} compounds, which could be attributed to the cross-products of n-heptylcyclohexane and α-pinene oxidation and their intermediates, leading to the formation of high carbon number compounds. However, upon the addition of NH_3, it promoted the transformation of high molecular weight products into smaller ones, resulting in a decrease in the abundance of C_{11} to C_{15}. This was consistent with the previous conclusion.

3.3.3 Compounds composition

Furthermore, we identify SOA compounds by dividing regions based on different O/C, H/C, and OSC values. (Fig. 8). Given that the reaction precursors did not contain aromatic compounds, naturally no aromatic hydrocarbons were formed in region A1. Clearly under the positive mode, the products of n-heptylcyclohexane and α-pinene were mainly found in region A2 and B1, suggesting that the products from both single and mixed systems were primarily composed of aliphatic compounds and oxygenated organic molecules (OOMs) with more reducing functional groups. Scaling by nitrogen number allows for a more intuitive view of the NOC species distribution. Since the SOA collected in this experiment covered entire reaction period, it might contain some intermediates with unstable structures. Furthermore, the oxidation conditions in our photochemical experiments were significantly more complex than those in the ozonolysis of single α-pinene. Consequently, the average H:C ratio was likely to be slightly higher than reference values (Putman et al., 2012). In the presence of NH_3, there were fewer compounds in B2 than in the experiments without NH_3 (Fig. S2) presenting fewer OOMs with more oxidizing functional groups (alcohols, ethers, peroxides, carbonyls) in the products. This could be attributed to the suppression effect

of OOMs formation by NH₃. As for the negative mode, the products of n-heptylcyclohexane and α-pinene were major

310   detected as aliphatic compounds (Fig. S3 and S4). Furthermore, the mass defect plot revealed that products bearing a higher oxygen content were clearly detected in the absence of NH₃, whereas the maximum oxygen content of the products was markedly lower when NH₃ was present, implying that NH₃ could terminate the multistep oxidation of oligomeric intermediates during the reaction (Fig. S5 and S6). This also suggested that the presence of NH₃ inhibited the formation of OOMs. In summary, the photo-oxidation reaction of the n-heptylcyclohexane and α-pinene single / mixed systems yielded

315   aliphatic compounds and OOMs, and the participation of NH₃ in the reaction could suppress the formation of OOMs.
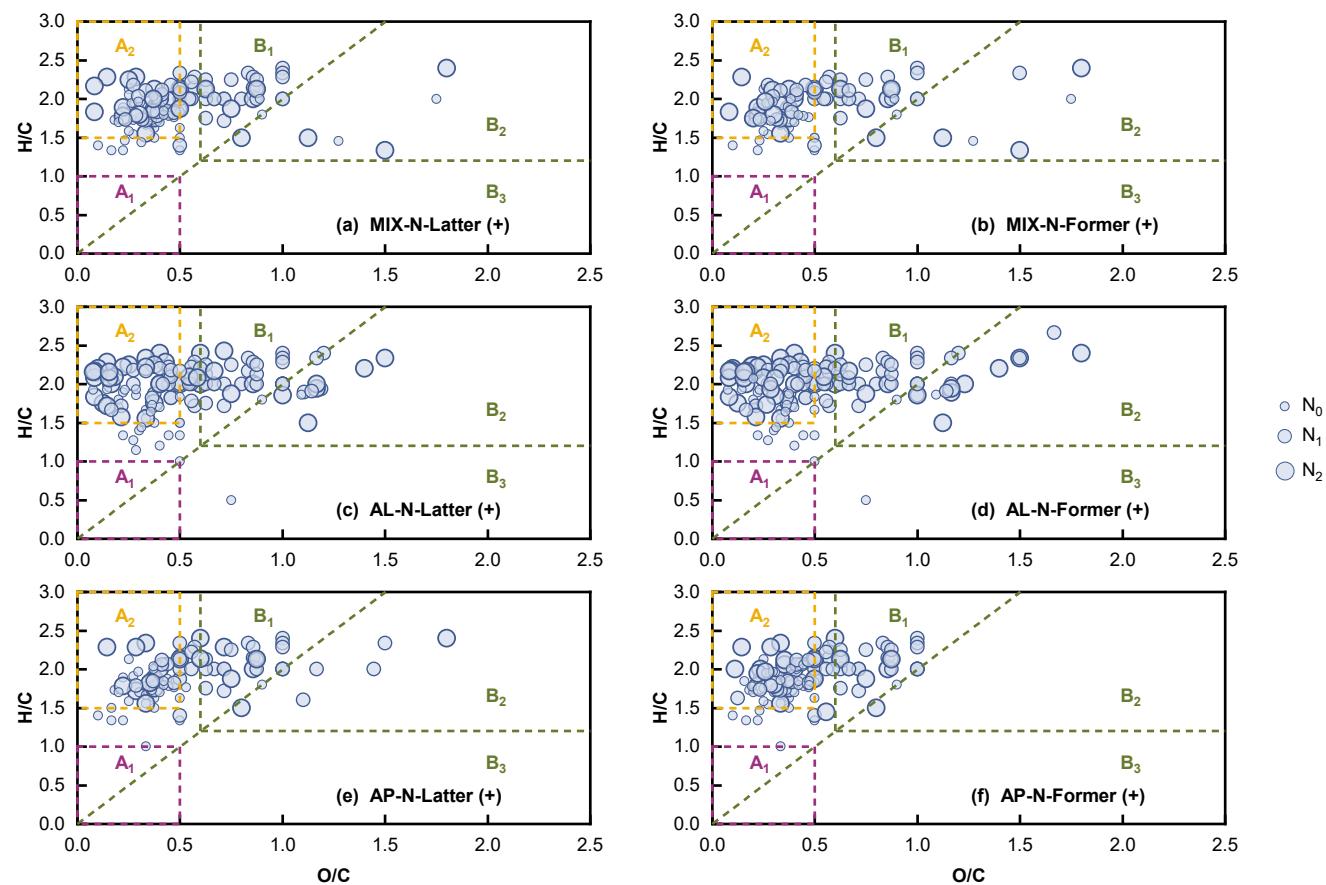
Figure 8. Van Krevelen diagram of compounds detected single / mixed experiments of n-heptylcyclohexane and α-pinene under positive mode. The lower left region (Al) with low H/C and low O/C region (O/C ≤ 0.5, H/C ≤ 1.0) indicated the low oxygen aromatic hydrocarbons. The region A2 with high H/C and low O/C region (O/C ≤ 0.5, H/C ≥ 1.5) represented aliphatic compounds

320   **(Mazzoleni et al.,2010; Mazzoleni et.al,.2012). OOMs contained a great fraction of reducing functional groups in the Bl region (O/C ≥ 0.6, H/C > 1.2, OSc < 0), oxidizing functional groups in the B2 region (O/C ≥ 0.6, H/C > 1.2, OSc > 0). The moderate oxidation level OOMs were in B3 region (OSc ≥ 0, H/C ≤ 1.2) (Tu et.al.,.2016)**

3.4 Generation of OVOCs Intermediates

To gain a more comprehensive understanding of the mechanisms of SOA formation, we conducted an analysis of

325   oxygenated VOCs (OVOCs) intermediates, key carbonyl compounds identified in the reaction products (Fig. 9). In the MIX

experiment, hexanal peaked at 1.1 μg m^{-3} during the former half of the reaction, and was subsequently consumed by fragmentation or further oxidation. The highest concentration in the latter half of the reaction was heptanal (2.3 μg m^{-3}), which could be attributed to the fact that the heptane branch was first broken and further oxidation was required to break into smaller branches, but sufficient oxidation environment cannot be provided by largely consumed oxidants in the later stage of

330 the reaction. In this system, the total amount of aldehydes and ketones was relatively small, presumably because the aldehydes/ketones reacted with intermediates or products and were transferred to the particle phase. When NH_3 was present, the mass concentrations of all carbonyls rose sharply, indicating that NH_3 either initiated cross reactions and side-reactions within the mixture or reacted with specific intermediates, driving more oxidation/fragmentation of the intermediates into aldehydes and ketones.

335 In the AL experiment, every carbonyl except crotonaldehyde and heptanal was more abundant in the latter half of the reaction. This might be due to the unstable structure of these two compounds, which caused their rapid oxidation to other substances. Moreover, relative to the NH_3-free case, the NH_3-present system produced substantially more aldehydes and ketones with ≤4 carbon atoms, demonstrating that NH_3 enhanced carbonyl compounds formation in the system, especially that with small molecule.

340 In the AP experiment, compared with the NH_3-free system, every carbonyl except acetaldehyde increased when NH_3 was present. The decrease of acetaldehyde presumably because NH_3 reacted directly with it to form nitrogen-containing products that partitioned into the particle phase, lowering its gas-phase concentration.

In summary, NH_3 redirected the oxidation pathway through competitive reactions, yielding a larger fraction of lower molecular weight products and small carbonyls.
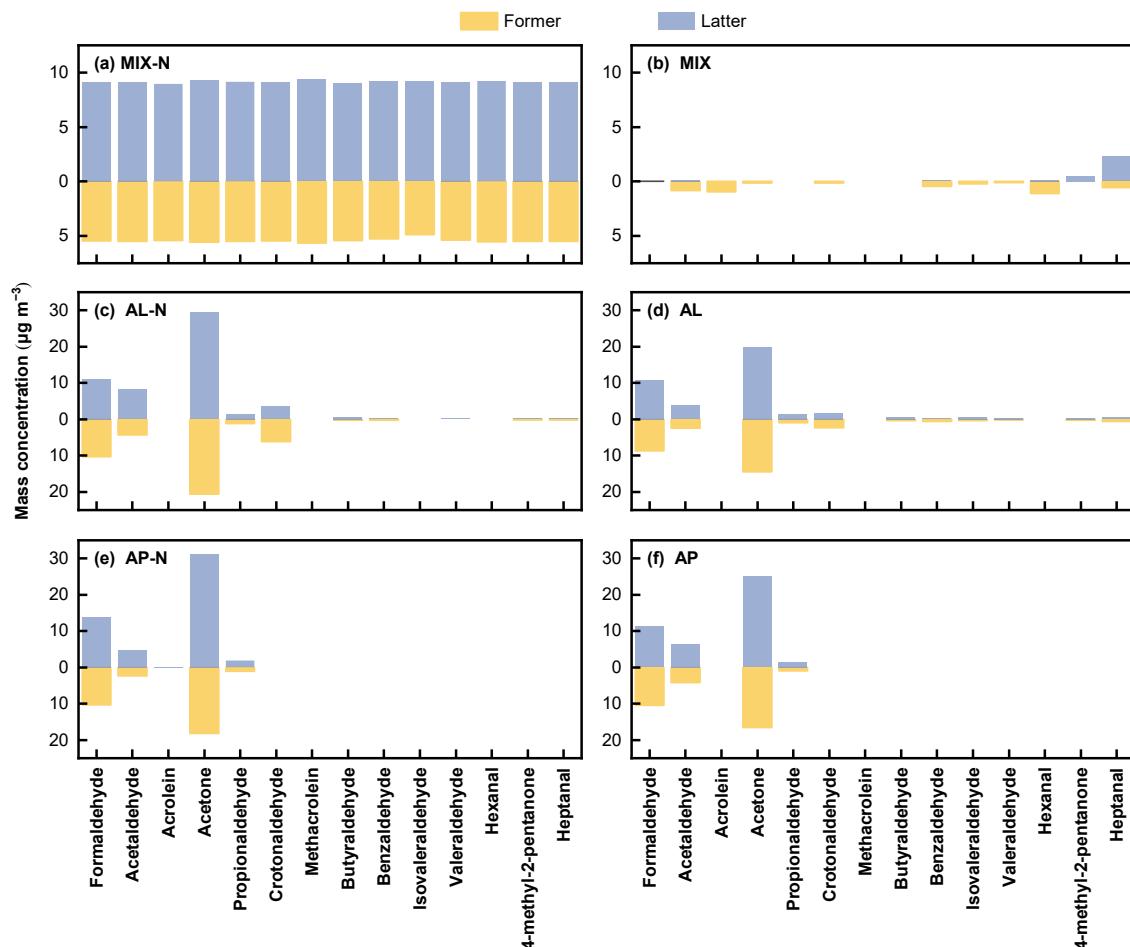
Figure 9. Mass concentration of aldehydes and ketones generated by photo oxidation in the (a) MIX-N (n-heptylcyclohexane + α-pinene + HONO + NH₃) experiment, (b) MIX (n-heptylcyclohexane + α-pinene + HONO) experiment, (c) AL-N (n-heptylcyclohexane + HONO + NH₃), (d) AL (n-heptylcyclohexane + HONO) experiment, (e) AP-N (α-pinene + HONO + NH₃) experiment and (f) AP (α-pinene + HONO) experiment.

3.5 Possible photochemical oxidation paths

Under high-NOx conditions, the photo-oxidation reaction of n-heptylcyclohexane and α-pinene mixture began with H-abstraction by OH radical and thus reaction with O_2 to form an alkyl peroxy radical (RO_2). When NH_3 co-existed with n-heptylcyclohexane, α-pinene and NOx, it markedly enhanced SOA production from the photochemical oxidation of the binary mixture. Cross-reactions between n-heptylcyclohexane, α-pinene and their organic intermediates promoted nucleation and growth of high-molecular-weight oligomers; in particular, peroxy radicals derived from n-heptylcyclohexane added across the double bond of α-pinene, yielding mixed oxidation products such as alkylated terpene oxides. Concurrently, NH_3 neutralised organic acids to form low-volatility ammonium salts, strongly depressing their saturation vapour pressures. NH_3 also reacted with OH radicals or organic radicals to generate nitrogen-containing radicals that further evolved into N-

containing molecules, again lowering volatility. Moreover, NH₃ participated in Maillard chemistry with carbonyls, producing
360   N-heterocycles (e.g. imidazoles, Fig. 10) that subsequently fragmented into smaller N-heterocycles and organic acids.
Existing observational evidence had indicated that the presence of NH₃ could substantially enhance the formation of
imidazole compounds (Liu et al., 2023). These low-volatility products underwent further multigenerational oxidation, giving
highly oxygenated and nitrated species. Through these intertwined pathways NH₃ substantially reduced the overall volatility
of the photo-oxidation products from the n-heptylcyclohexane and α-pinene mixture, efficiently enhancing SOA formation.
365   By reacting with organic peroxy radicals formed during oxidation, NH₃ produced low volatility compounds that partitioned
directly into the particle phase. This partitioning interrupted self-/cross-reactions of RO₂· and suppressed the formation of
large OOMs. Meanwhile, multi-step oxidation initiated by NH₃ reacting with carbonyls additionally generated aldehydic and
ketonic intermediates, further enriching the gas-phase carbonyl compounds.
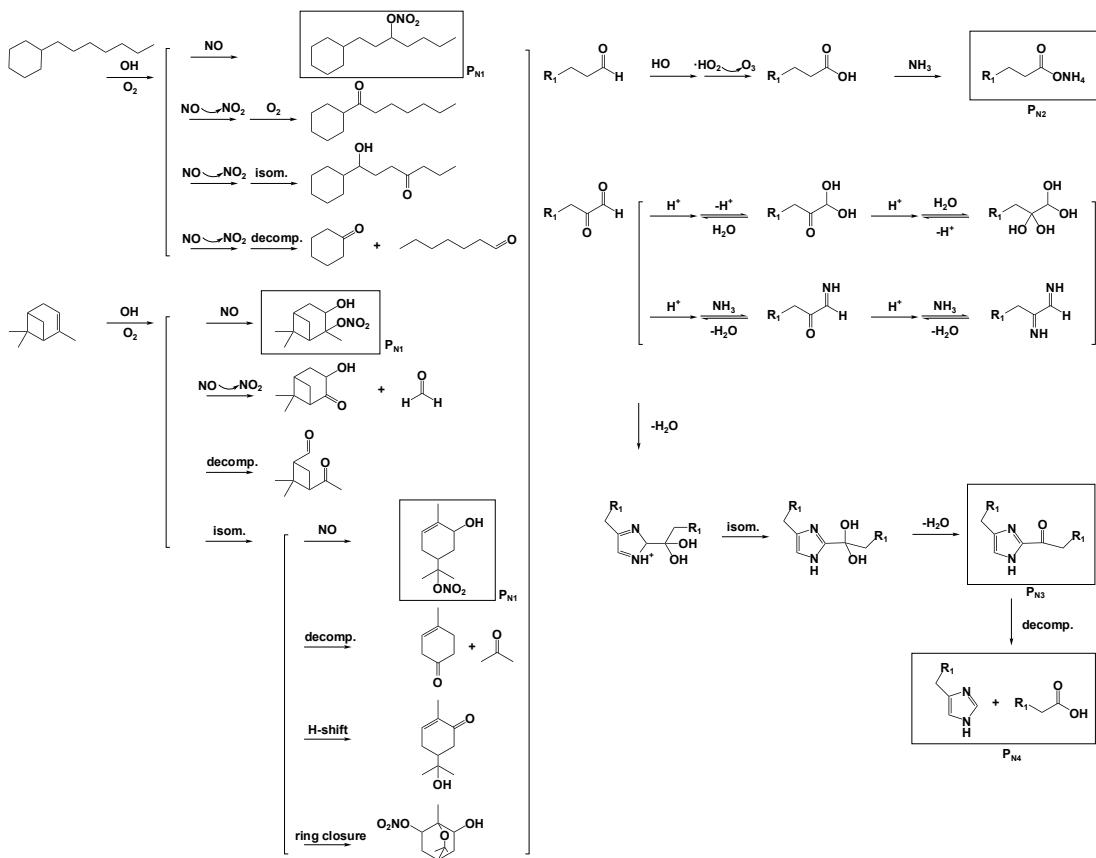
370   **Figure 10. Proposed possible reactions of the mixture experiment in the presence of NH₃ (R₁ was alkyl groups, P_{N1} was organic nitrate esters, P_{N2} was organic ammonium salt, P_{N3} was imidazole compounds, P_{N4} was multi-generational compounds of imidazole cleavage).**

4 Conclusions

In the present work, a large-scale outdoor photochemical smog chamber was utilized to study the effect of inorganic gases
(NH$_3$) on the photochemical process of mixed AVOC (n-heptylcyclohexane) and BVOC (α-pinene). After the reaction
begins, NH$_3$ promoted nucleation and participated in particle-phase reactions, leading to the rapid formation and growth of
SOA particles within one hour, consequently accelerating precursor consumption. In contrast to previous findings, the
influence of NH$_3$ on the surface mean particle size of precursor-derived SOA was relatively small, primarily because a
higher VOC/NOx ratio could weaken the enhancement of new particle growth under high-NOx conditions. The primary
products from experiments with mixed n-heptylcyclohexane and α-pinene were gas-phase carbonyl compounds, as well as
particle-phase aliphatic compounds, NOCs including imidazoles, and oxygenated organic molecules (OOMs). Reactions
between NH$_3$ and carbonyls enhanced the production of aldehydes and ketones, while its acid-base reactions with organic
acids, its radical reactions, and its Maillard reactions with carbonyls promoted SOA formation in the binary system.
Furthermore, reactions between NH$_3$ and organic radicals terminated the cross-reactions and autoxidation of RO$_2$, thereby
suppressing OOMs formation.

This study explored the influence of NH$_3$ on photochemical oxidation reactions and products in mixed systems of cyclic
branched alkanes and biogenic alkenes under high-NOx conditions, improving upon previous studies of single organic
systems by better simulating real atmospheric conditions. The findings can deepen the understanding of SOA formation in
regions impacted by complex emissions and further clarify the mechanisms through which NH$_3$ affects mixed oxidation
reactions. This study reveals potential pathways for NH$_3$ participation in mixed oxidation reactions. Future research should
conduct in-depth analyses and quantification of product characteristics to elucidate definite pathways, thereby achieving a
comprehensive understanding of chem-physical processes in the real atmosphere.

In recent years, global NH$_3$ emissions have shown an overall upward trend, with agricultural emissions remaining dominant.
South and East Asia (e.g., India, Bangladesh, and China) are regions with the highest global NH$_3$ concentrations, while
significant concentrations have also been observed in biomass burning areas of North Africa, Central Africa, and South
America (Khan et al., 2020). Because NH$_3$ influences aerosol formation and evolution in multiple ways, investigating its
atmospheric behavior and accurately identifying its chemical evolution mechanisms in complex atmospheric environments
can help to mitigate aerosol impacts on climate and improve the accuracy of regional air quality forecasting.

Data availability

The data used in this study are available upon request from the corresponding author.

Acknowledgements

This work was financially supported by the National Natural Science Foundation of China (42405104), National Key Research and Development Program of China (No. 2024YFC3712902), the National Natural Science Foundation of China (42130606, 42175133, 22306179). The authors thank Mr. Chunshan Liu of Beijing Convenient Environmental Tech Co. Ltd
405 (http://www.bjkwnt.com/) for their help and support in smog chamber setup.

Author contributions

J.L. conceived the study. Y.Y. performed the experiments and conducted the data analyses. Y.Y. and J.L. interpreted and discussed the data results. Y.Y. wrote the manuscript. J.L. and H.L. revised the manuscript. All authors contributed to the final paper.

410 **Competing interests**

The authors declare no competing interests.

References

Agrawal, H., Sawant, A. A., Jansen, K., Miller, J. W., and Cocker, D. R.: Characterization of chemical and particulate
415 emissions from aircraft engines, Atmospheric Environment, 42, 4380-4392, 10.1016/j.atmosenv.2008.01.069, 2008.
Ahlberg, E., Falk, J., Eriksson, A., Holst, T., Brune, W. H., Kristensson, A., Roldin, P., and Svenningsson, B.: Secondary organic aerosol from VOC mixtures in an oxidation flow reactor, Atmospheric Environment, 161, 210-220, 10.1016/j.atmosenv.2017.05.005, 2017.
Atkinson, R. and Arey, J.: Atmospheric Degradation of Volatile Organic Compounds, Chemical Reviews, 103, 4605−4638,
420 2003.
Babar, Z. B., Park, J.-H., and Lim, H.-J.: Influence of NH3 on secondary organic aerosols from the ozonolysis and photooxidation of α-pinene in a flow reactor, Atmospheric Environment, 164, 71-84, 10.1016/j.atmosenv.2017.05.034, 2017.
Capouet, M., Peeters, J., Nozière, B., and Müller, J. F.: Alpha-pinene oxidation by OH: simulations of laboratory experiments, Atmospheric Chemistry and Physics, 4, 2285-2311, 10.5194/acp-4-2285-2004, 2004.
425 Chen, T. and Jang, M.: Secondary organic aerosol formation from photooxidation of a mixture of dimethyl sulfide and isoprene, Atmospheric Environment, 46, 271-278, 10.1016/j.atmosenv.2011.09.082, 2012.
Cui, Y., Chen, K., Zhang, H., Lin, Y. H., and Bahreini, R.: Chemical Composition and Optical Properties of Secondary Organic Aerosol from Photooxidation of Volatile Organic Compound Mixtures, ACS EST Air, 1, 247-258, 10.1021/acsestair.3c00041, 2024.
430 Deng, W., Liu, T. Y., Zhang, Y. L., Situ, S. P., Hu, Q. H., He, Q. F., Zhang, Z., Lü, S. J., Bi, X. H., Wang, X. M., Boreave, A., George, C., Ding, X., and Wang, X. M.: Secondary organic aerosol formation from photo-oxidation of toluene with NOx and SO2: Chamber simulation with purified air versus urban ambient air as matrix, Atmospheric Environment, 150, 67-76, 10.1016/j.atmosenv.2016.11.047, 2017a.

Deng, W., Hu, Q., Liu, T., Wang, X., Zhang, Y., Song, W., Sun, Y., Bi, X., Yu, J., Yang, W., Huang, X., Zhang, Z., Huang,
Z., He, Q., Mellouki, A., and George, C.: Primary particulate emissions and secondary organic aerosol (SOA) formation
from idling diesel vehicle exhaust in China, Sci Total Environ, 593-594, 462-469, 10.1016/j.scitotenv.2017.03.088, 2017b.

Donahue, N. M., Robinson, A. L., and Pandis, S. N.: Atmospheric organic particulate matter: From smoke to secondary
organic aerosol, Atmospheric Environment, 43, 94-106, 10.1016/j.atmosenv.2008.09.055, 2009.

Donahue, N. M., Robinson, A. L., Stanier, C. O., and Pandis, S. N.: Coupled partitioning, dilution, and chemical aging of
semivolatile organics, Environmental Science & Technology, 40, 2635-2643, 10.1021/es052297c, 2006.

Du, L., Xu, L., Li, K., George, C., and Ge, M.: NH3 Weakens the Enhancing Effect of SO2 on Biogenic Secondary Organic
Aerosol Formation, Environmental Science & Technology Letters, 10, 145-151, 10.1021/acs.estlett.2c00959, 2023.

Emanuelsson, E. U., Hallquist, M., Kristensen, K., Glasius, M., Bohn, B., Fuchs, H., Kammer, B., Kiendler-Scharr, A., Nehr,
S., Rubach, F., Tillmann, R., Wahner, A., Wu, H. C., and Mentel, T. F.: Formation of anthropogenic secondary organic
aerosol (SOA) and its influence on biogenic SOA properties, Atmospheric Chemistry and Physics, 13, 2837-2855,
10.5194/acp-13-2837-2013, 2013.

Fang, H., Huang, X., Zhang, Y., Pei, C., Huang, Z., Wang, Y., Chen, Y., Yan, J., Zeng, J., Xiao, S., Luo, S., Li, S., Wang, J.,
Zhu, M., Fu, X., Wu, Z., Zhang, R., Song, W., Zhang, G., Hu, W., Tang, M., Ding, X., Bi, X., and Wang, X.: Measurement
report: Emissions of intermediate-volatility organic compounds from vehicles under real-world driving conditions in an
urban tunnel, Atmospheric Chemistry and Physics, 21, 10005-10013, 10.5194/acp-21-10005-2021, 2021.

Hallquist, M., Wenger, J. C., Baltensperger, U., Rudich, Y., Simpson, D., Claeys, M., Dommen, J., Donahue, N. M., George,
C., Goldstein, A. H., Hamilton, J. F., Herrmann, H., Hoffmann, T., Iinuma, Y., Jang, M., Jenkin, M. E., Jimenez, J. L.,
Kiendler-Scharr, A., Maenhaut, W., McFiggans, G., Mentel, T. F., Monod, A., Prévôt, A. S. H., Seinfeld, J. H., Surratt, J. D.,
Szmigielski, R., and Wildt, J.: The formation, properties and impact of secondary organic aerosol: current and emerging
issues, Atmospheric Chemistry and Physics, 9, 5155-5236, 10.5194/acp-9-5155-2009, 2009.

Hao, L. Q., Kari, E., Leskinen, A., Worsnop, D. R., and Virtanen, A.: Direct contribution of ammonia to α-pinene secondary
organic aerosol formation, Atmospheric Chemistry and Physics, 20, 14393-14405, 10.5194/acp-20-14393-2020, 2020.

Hu, W., Zhou, H., Chen, W., Ye, Y., Pan, T., Wang, Y., Song, W., Zhang, H., Deng, W., Zhu, M., Wang, C., Wu, C., Ye, C.,
Wang, Z., Yuan, B., Huang, S., Shao, M., Peng, Z., Day, D. A., Campuzano-Jost, P., Lambe, A. T., Worsnop, D. R., Jimenez,
J. L., and Wang, X.: Oxidation Flow Reactor Results in a Chinese Megacity Emphasize the Important Contribution of
S/IVOCs to Ambient SOA Formation, Environ Sci Technol, 56, 6880-6893, 10.1021/acs.est.1c03155, 2022.

Huang, M., Xu, J., Cai, S., Liu, X., Hu, C., Gu, X., Zhao, W., Fang, L., and Zhang, W.: Chemical analysis of particulate
products of aged 1,3,5-trimethylbenzene secondary organic aerosol in the presence of ammonia, Atmospheric Pollution
Research, 9, 146-155, 10.1016/j.apr.2017.08.003, 2018.

John H. Offenberg, Charles W. Lweis, Michael Lewandowski, Mohammed Jaoui, Tadeusz E. Kleindienst, and Edney, E. O.:
Contributions of toluene and α-Pinene to SOA formed in an irradiated toluene/α-pinene/NOx/ air mixture: Comparison of
results using 14C content and SOA organic tracer methods, Environmental Science & Technology 41, 3972-3976, 2007.

Khan, M. A. H., Lowe, D., Derwent, R. G., Foulds, A., Chhantyal-Pun, R., McFiggans, G., Orr-Ewing, A. J., Percival, C. J.,
and Shallcross, D. E.: Global and regional model simulations of atmospheric ammonia, Atmospheric Research, 234,
10.1016/j.atmosres.2019.104702, 2020.

Lambe, A. T., Onasch, T. B., Croasdale, D. R., Wright, J. P., Martin, A. T., Franklin, J. P., Massoli, P., Kroll, J. H.,
Canagaratna, M. R., Brune, W. H., Worsnop, D. R., and Davidovits, P.: Transitions from Functionalization to Fragmentation
Reactions of Laboratory Secondary Organic Aerosol (SOA) Generated from the OH Oxidation of Alkane Precursors,
Environ. Sci. Technol., 46, 5430-5437, 10.1021/es300274t, 2012.

Laskin, A., Laskin, J., and Nizkorodov, S. A.: Chemistry of Atmospheric Brown Carbon, Chemical Reviews, 115, 4335-
4382, 10.1021/cr5006167, 2015.

Li, J., Xu, W., You, B., and Sun, Y.: Dynamic variations of ammonia in various life spaces and seasons and the influences of
human activities, Building and Environment, 212, 10.1016/j.buildenv.2022.108820, 2022a.

Li, J., Li, K., Li, H., Wang, X., Wang, W., Wang, K., and Ge, M.: Long-chain alkanes in the atmosphere: A review, J
Environ Sci (China), 114, 37-52, 10.1016/j.jes.2021.07.021, 2022b.

Li, J., Li, K., Li, H., Wang, X., Wang, W., Wang, K., and Ge, M.: Long-chain alkanes in the atmosphere: A review, Journal
of Environmental Sciences, 114, 37-52, 10.1016/j.jes.2021.07.021, 2022c.

Li, J., Li, H., Li, K., Chen, Y., Zhang, H., Zhang, X., Wu, Z., Liu, Y., Wang, X., Wang, W., and Ge, M.: Enhanced secondary organic aerosol formation from the photo-oxidation of mixed anthropogenic volatile organic compounds,
485 Atmospheric Chemistry and Physics, 21, 7773-7789, 10.5194/acp-21-7773-2021, 2021a.

Li, J., Li, H., Wang, X., Wang, W., Ge, M., Zhang, H., Zhang, X., Li, K., Chen, Y., Wu, Z., Chai, F., Meng, F., Mu, Y., Mellouki, A., Bi, F., Zhang, Y., Wu, L., and Liu, Y.: A large-scale outdoor atmospheric simulation smog chamber for studying atmospheric photochemical processes: Characterization and preliminary application, Journal of Environmental Sciences, 102, 185-197, 10.1016/j.jes.2020.09.015, 2021b.

490 Li, J., Li, K., Zhang, H., Zhang, X., Ji, Y., Chu, W., Kong, Y., Chu, Y., Ren, Y., Zhang, Y., Zhang, H., Gao, R., Wu, Z., Bi, F., Chen, X., Wang, X., Wang, W., Li, H., and Ge, M.: Effects of OH radical and SO2 concentrations on photochemical reactions of mixed anthropogenic organic gases, Atmospheric Chemistry and Physics, 22, 10489-10504, 10.5194/acp-22-10489-2022, 2022d.

Li, K., Chen, L., White, S. J., Yu, H., Wu, X., Gao, X., Azzi, M., and Cen, K.: Smog chamber study of the role of NH3 in
495 new particle formation from photo-oxidation of aromatic hydrocarbons, Sci Total Environ, 619-620, 927-937, 10.1016/j.scitotenv.2017.11.180, 2018.

Li, K., Zhang, J., Bell, D. M., Wang, T., Lamkaddam, H., Cui, T., Qi, L., Surdu, M., Wang, D., Du, L., El Haddad, I., Slowik, J. G., and Prevot, A. S. H.: Uncovering the dominant contribution of intermediate volatility compounds in secondary organic aerosol formation from biomass-burning emissions, Natl Sci Rev, 11, nwae014, 10.1093/nsr/nwae014, 2024.

500 Liu, F., Xu, T., Ng, N. L., and Lu, H.: Linking Cell Health and Reactive Oxygen Species from Secondary Organic Aerosols Exposure, Environ. Sci. Technol., 57, 1039-1048, 10.1021/acs.est.2c05171, 2022.

Liu, S., Huang, D., Wang, Y., Zhang, S., Liu, X., Wu, C., Du, W., and Wang, G.: Synergetic effects of NH3 and NOx on the production and optical absorption of secondary organic aerosol formation from toluene photooxidation, Atmospheric Chemistry and Physics, 21, 17759-17773, 10.5194/acp-21-17759-2021, 2021a.

505 Liu, S., Wang, Y., Wang, G., Zhang, S., Li, D., Du, L., Wu, C., Du, W., and Ge, S.: Enhancing effect of NO2 on the formation of light-absorbing secondary organic aerosols from toluene photooxidation, Science of the Total Environment, 794, 148714, 10.1016/j.scitotenv.2021.148714, 2021b.

Liu, T., Wang, X., Wang, B., Ding, X., Deng, W., Lu, S., and Zhang, Y.: Emission factor of ammonia (NH$_3$) from on-road vehicles in China: tunnel tests in urban Guangzhou, Environmental Research Letters, 9, 10.1088/1748-
510 9326/9/6/064027, 2014.

Liu, X. D., Wang, H. Y., Wang, F. L., Lv, S. J., Wu, C., Zhao, Y., Zhang, S., Liu, S. J., Xu, X. B., Lei, Y. L., and Wang, G. H.: Secondary Formation of Atmospheric Brown Carbon in China Haze: Implication for an Enhancing Role of Ammonia, Environmental Science & Technology, 57, 11163-11172, 10.1021/acs.est.3c03948, 2023.

Liu, Y., Liggio, J., Staebler, R., and Li, S. M.: Reactive uptake of ammonia to secondary organic aerosols: kinetics of
515 organonitrogen formation, Atmospheric Chemistry and Physics, 15, 13569-13584, 10.5194/acp-15-13569-2015, 2015.

Luo, H., Jia, L., Wan, Q., An, T. C., and Wang, Y. J.: Role of liquid water in the formation of O$_3$ and SOA particles from 1,2,3-trimethylbenzene, Atmospheric Environment, 217, 10.1016/j.atmosenv.2019.116955, 2019.

Mao, J., Ren, X., Brune, W. H., Olson, J. R., Crawford, J. H., Fried, A., Huey, L. G., Cohen, R. C., Heikes, B., Singh, H. B., Blake, D. R., Sachse, G. W., Diskin, G. S., Hall, S. R., and Shetter, R. E.: Airborne measurement of OH reactivity during
520 INTEX-B, Atmos. Chem. Phys., 9, 163-173, 10.5194/acp-9-163-2009, 2009.

Martinez, R. D., Buitrago, A. A., Howell, N. W., Hearn, C. H., and Joens, J. A.: THE NEAR UV ABSORPTION-SPECTRA OF SEVERAL ALIPHATIC-ALDEHYDES AND KETONES AT 300-K, Atmospheric Environment Part a-General Topics, 26, 785-792, 10.1016/0960-1686(92)90238-g, 1992.

Ming, L., Jin, L., Li, J., Fu, P., Yang, W., Liu, D., Zhang, G., Wang, Z., and Li, X.: PM2.5 in the Yangtze River Delta, China:
525 Chemical compositions, seasonal variations, and regional pollution events, Environmental Pollution, 223, 200-212, 10.1016/j.envpol.2017.01.013, 2017.

O'Brien, R. E., Laskin, A., Laskin, J., Liu, S., Weber, R., Russell, L. M., and Goldstein, A. H.: Molecular characterization of organic aerosol using nanospray desorption/electrospray ionization mass spectrometry: CalNex 2010 field study, Atmospheric Environment, 68, 265-272, 10.1016/j.atmosenv.2012.11.056, 2013.

530 Palm, B. B., Campuzano-Jost, P., Day, D. A., Ortega, A. M., Fry, J. L., Brown, S. S., Zarzana, K. J., Dube, W., Wagner, N. L., Draper, D. C., Kaser, L., Jud, W., Karl, T., Hansel, A., Gutiérrez-Montes, C., and Jimenez, J. L.: Secondary organic

aerosol formation from in situ OH, O3 and NO3 oxidation of ambient forest air in an oxidation flow reactor, Atmospheric Chemistry and Physics, 17, 5331-5354, 10.5194/acp-17-5331-2017, 2017.

535 Putman, A. L., Offenberg, J. H., Fisseha, R., Kundu, S., Rahn, T. A., and Mazzoleni, L. R.: Ultrahigh-resolution FT-ICR mass spectrometry characterization of α-pinene ozonolysis SOA, Atmospheric Environment, 46, 164-172, 10.1016/j.atmosenv.2011.10.003, 2012.

Qi, L., Liu, H., Shen, X., Fu, M., Huang, F., Man, H., Deng, F., Shaikh, A. A., Wang, X., Dong, R., Song, C., and He, K.: Intermediate-Volatility Organic Compound Emissions from Nonroad Construction Machinery under Different Operation Modes, Environ Sci Technol, 53, 13832-13840, 10.1021/acs.est.9b01316, 2019.

540 Roach, P. J., Laskin, J., and Laskin, A.: Higher-Order Mass Defect Analysis for Mass Spectra of Complex Organic Mixtures, Anal. Chem., 83, 4924-4929, 10.1021/ac200654j, 2011.

Shao, Y., Voliotis, A., Du, M., Wang, Y., Pereira, K., Hamilton, J., Alfarra, M. R., and McFiggans, G.: Chemical composition of secondary organic aerosol particles formed from mixtures of anthropogenic and biogenic precursors, Atmospheric Chemistry and Physics, 22, 9799-9826, 10.5194/acp-22-9799-2022, 2022.

545 Shrivastava, M., Cappa, C. D., Fan, J., Goldstein, A. H., Guenther, A. B., Jimenez, J. L., Kuang, C., Laskin, A., Martin, S. T., Ng, N. L., Petaja, T., Pierce, J. R., Rasch, P. J., Roldin, P., Seinfeld, J. H., Shilling, J., Smith, J. N., Thornton, J. A., Volkamer, R., Wang, J., Worsnop, D. R., Zaveri, R. A., Zelenyuk, A., and Zhang, Q.: Recent advances in understanding secondary organic aerosol: Implications for global climate forcing, Reviews of Geophysics, 55, 509-559, 10.1002/2016rg000540, 2017.

550 Siegl, W. O., Hammerle, R. H., Herrmann, H. M., Wenclawiak, B. W., and Luers-Jongen, B.: Organic emissions profile for a light-duty diesel vehicle, Atmospheric Environment, 33, 797-805, 10.1016/s1352-2310(98)00209-x, 1999.

Sun, K., Tao, L., Miller, D. J., Pan, D., Golston, L. M., Zondlo, M. A., Griffin, R. J., Wallace, H. W., Leong, Y. J., Yang, M. M., Zhang, Y., Mauzerall, D. L., and Zhu, T.: Vehicle Emissions as an Important Urban Ammonia Source in the United States and China, Environ. Sci. Technol., 51, 2472-2481, 10.1021/acs.est.6b02805, 2017.

555 Tang, R. Z., Wang, H., Liu, Y., and Guo, S.: Constituents of Atmospheric Semi-Volatile and Intermediate Volatility Organic Compounds and Their Contribution to Organic Aerosol, Progress in Chemistry, 31, 180-190, 10.7536/pc180431, 2019.

Voliotis, A., Wang, Y., Shao, Y., Du, M., Bannan, T. J., Percival, C. J., Pandis, S. N., Alfarra, M. R., and McFiggans, G.: Exploring the composition and volatility of secondary organic aerosols in mixed anthropogenic and biogenic precursor systems, Atmospheric Chemistry and Physics, 21, 14251-14273, 10.5194/acp-21-14251-2021, 2021.

560 Wang, H., Guo, S., Yu, Y., Shen, R., Zhu, W., Tang, R., Tan, R., Liu, K., Song, K., Zhang, W., Zhang, Z., Shuai, S., Xu, H., Zheng, J., Chen, S., Li, S., Zeng, L., and Wu, Z.: Secondary aerosol formation from a Chinese gasoline vehicle: Impacts of fuel (E10, gasoline) and driving conditions (idling, cruising), Sci Total Environ, 795, 148809, 10.1016/j.scitotenv.2021.148809, 2021a.

WANG, K., WANG, W., LI, J., LIU, X., YANG, W., LI, J., and GE, M.: Research progress of intermediate volatility
565 organic compounds, Environmental Chemistry and Ecotoxicology, 40, 10.7524/j.issn.0254-6108.2021032906, 2021b.

Wang, Y., Liu, S., and Wang, G.: Effects of NH3 on the formation of SOA derived from xylene photochemical oxidation, Journal of Atmospheric and Environmental Optics, 17, 185-194, 2022.

Wen, Y., Zhang, S., Wu, Y., and Hao, J.: Vehicular ammonia emissions: an underappreciated emission source in densely populated areas, Atmospheric Chemistry and Physics, 23, 3819-3828, 10.5194/acp-23-3819-2023, 2023.

570 Xu, L., Du, L., Tsona, N. T., and Ge, M.: Anthropogenic Effects on Biogenic Secondary Organic Aerosol Formation, Advances in Atmospheric Sciences, 38, 1053-1084, 10.1007/s00376-020-0284-3, 2021.

Yuan, B., Hu, W. W., Shao, M., Wang, M., Chen, W. T., Lu, S. H., Zeng, L. M., and Hu, M.: VOC emissions, evolutions and contributions to SOA formation at a receptor site in eastern China, Atmospheric Chemistry and Physics, 13, 8815-8832, 10.5194/acp-13-8815-2013, 2013.

575 Zhang, P., Chen, T., Liu, J., Liu, C., Ma, J., Ma, Q., Chu, B., and He, H.: Impacts of SO2, Relative Humidity, and Seed Acidity on Secondary Organic Aerosol Formation in the Ozonolysis of Butyl Vinyl Ether, Environ. Sci. Technol., 53, 8845-8853, 10.1021/acs.est.9b02702, 2019.

Zhang, S., Du, L., Yang, Z., Tchinda, N. T., Li, J., and Li, K.: Contrasting impacts of humidity on the ozonolysis of monoterpenes: insights into the multi-generation chemical mechanism, Atmospheric Chemistry and Physics, 23, 10809-
580 10822, 10.5194/acp-23-10809-2023, 2023.

Ziemann, P. J. and Atkinson, R.: Kinetics, products, and mechanisms of secondary organic aerosol formation, Chemical Society Reviews, 41, 10.1039/c2cs35122f, 2012.